Molecular model of the ferroportin intracellular gate and implications for the human iron transport cycle and hemochromatosis type 4A

Julie Guellec, Ahmad Elbahnsi, Marlène Le Tertre, Kévin Uguen, Isabelle Gourlaouen, Claude Férec, Chandran Ka, Isabelle Callebaut, Gérald Le Gac

▶ **To cite this version:**

Julie Guellec, Ahmad Elbahnsi, Marlène Le Tertre, Kévin Uguen, Isabelle Gourlaouen, et al.. Molecular model of the ferroportin intracellular gate and implications for the human iron transport cycle and hemochromatosis type 4A. FASEB Journal, 2019, 33 (12), pp.14625-14635. 10.1096/fj.201901857R . hal-03031336

HAL Id: hal-03031336

https://hal.sorbonne-universite.fr/hal-03031336

Submitted on 30 Nov 2020

HAL is a multi-disciplinary open access archive for the deposit and dissemination of scientific research documents, whether they are published or not. The documents may come from teaching and research institutions in France or abroad, or from public or private research centers.

L'archive ouverte pluridisciplinaire **HAL**, est destinée au dépôt et à la diffusion de documents scientifiques de niveau recherche, publiés ou non, émanant des établissements d'enseignement et de recherche français ou étrangers, des laboratoires publics ou privés.

Molecular model of the ferroportin intracellular gate and implications for the human iron transport cycle and hemochromatosis type 4A

Running title: Ferroportin 1 structure and function.

Julie Guellec,[1,2] Ahmad Elbahnsi,[3] Marlène Le Tertre,[1,4] Kévin Uguen,[1,4] Isabelle Gourlaouen[1], Claude Férec[1,2,4], Chandran Ka,[1,4,5] Isabelle Callebaut[3*] and Gérald Le Gac[1,4,5*]

* IC and GLG contributed equally to this work

[1]INSERM UMR1078, Université Bretagne Loire – Université de Brest, Etablissement Français du Sang – Bretagne, Institut Brestois Santé-Agro-Matière, Brest, France; [2]Association Gaetan Saleun, Brest, France; [3] Sorbonne Université, Muséum National d'Histoire Naturelle, UMR CNRS 7590, Institut de Minéralogie, de Physique des Matériaux et de Cosmochimie, IMPMC, 75005 Paris, France; [4]Service de Génétique Médicale, CHRU de Brest, Hôpital Morvan, Brest, France; [5]Laboratory of Excellence GR-Ex, Paris, France.

Corresponding author:

Gerald LE GAC

Centre Hospitalier Regional Universitaire de Brest, Hôpital Morvan, Bat 5bis, Laboratoire de Genetique Moleculaire et d'Histocompatibilité, 2 Avenue Foch, 29200 Brest, France.
Phone: (+33) 2 98 44 50 64; e-mail: gerald.legac@univ-brest.fr.

Disclosure of Conflicts of Interest

The authors declare that they have no conflicts of interest.

Abstract

Ferroportin 1 (FPN1) is a Major Facilitator Superfamily (MFS) transporter that is essential for proper maintenance of human iron homeostasis at the systemic and cellular level. FPN1 dysfunction leads to the progressive accumulation of iron in reticuloendothelial cells, causing hemochromatosis type 4A (or ferroportin disease), an autosomal dominant disorder that displays large phenotypic heterogeneity. While crystal structures have unveiled the outward- and inward-facing conformations of the bacterial homolog BbFpn (or Bd2019), and calcium has recently been identified as an essential cofactor, our molecular understanding of the iron transport mechanism remains incomplete. Here, we used a combination of molecular modeling, molecular dynamics simulations and alanine site-directed mutagenesis, followed by complementary *in vitro* functional analyses, to explore the structural architecture of the human FPN1 intracellular gate. We reveal an inter-domain network that involves five key amino acids and is likely very important for stability of the iron exporter facing the extracellular milieu. We also identify inter- and intra-domain interactions that rely on the two Asp84 and Asn174 critical residues and do not exist in the bacterial homologue. These interactions are thought to play an important role in the modulation of conformational changes during the transport cycle. We interpret these results in the context of hemochromatosis type 4A, reinforcing the idea that different categories of loss-of-function mutations exist. Our findings provide an unprecedented view of the human FPN1 outward-facing structure and the particular function of the so-called “gating residues” in the mechanism of iron export.

Introduction

Ferroportin 1 (FPN1, also referred to as SLC40A1; Uniprot accession number Q9NP59) is the only known iron exporter in mammals and is considered to be a key player in both cellular and systemic iron homeostasis.(1–3) FPN1 is expressed in all types of cells that handle major iron flow, including macrophages, duodenal enterocytes, hepatocytes and placenta syncytiotrophoblasts.(4) Cell-surface expression is predominantly regulated by the liver-derived peptide hepcidin,(5) which induces internalization and degradation of FPN1, decreasing iron delivery to plasma.(2) The hepcidin-ferroportin axis plays an important role in the pathogenesis of inherited and acquired iron metabolism disorders, including iron overload diseases and iron-restricted anemia.(6)

FPN1 dysfunction is responsible for hemochromatosis type 4, an inborn error of iron metabolism that is transmitted as an autosomal dominant trait, and is characterized by wide clinical heterogeneity. This is only partially explained by the existence of mutations with opposing effects. Patients with loss-of-function mutations usually present mesenchymal or mixed iron overload (corresponding to early iron deposition within Kupffer cells) and markedly elevated serum ferritin concentrations contrasting with normal or transferrin saturation levels. This phenotypic presentation is commonly referred to as ferroportin disease, or hemochromatosis type 4A. Gain-of-function mutations, which are less frequent, result in partial to complete resistance to hepcidin; patients usually display elevated transferrin saturation levels. Hyperferritinemia is secondary to plasma iron burden and is mostly associated with iron deposits in hepatocytes. These biological and histological features mimic the natural history of *HFE*-related hemochromatosis; hence, gain-of-function FPN1 mutations are associated with hemochromatosis type 4B.

Important progress has been made these last five years in understanding FPN1 structural biology. We and others first provided evidence of the relatedness of FPN1 to the Major Facilitator Superfamily (MFS).(7–9) The MFS structural core consists of twelve transmembrane (TM) helices organized into two structurally similar domains: N-domain (TM1-TM6) and C-domain (TM7-TM12).(10) Taniguchi *et al.* then identified Bd2019 (BbFpn: *Bdellovibrio bacteriovorus* ferroportin(11)) as a bacterial homologue of the human iron exporter and solved its structures in both the outward- and inward-facing states.(12) The X-ray structures of BbFpn confirmed the typical MFS fold and provided important clues about the mechanism of iron egress and FPN1 regulation by hepcidin. Deshpande *et al.* very recently reported the crystal structure of Ca^{2+}-bound BbFpn in an inward-facing conformation and demonstrated that human FPN1 iron transport activity is dependent on extracellular Ca^{2+}.(13) The authors proposed an alternate access mechanism, which is

characteristic of MFS transporters,(10,14) to explain how iron is exported by FPN1 across the plasma membrane, comprising three fundamental steps: (1) in the outward-facing structure, Ca^{2+} binds to FPN1 and initiates a conformational change that enables transition from open outward-facing to open inward-facing states; (2) in the inward-facing structure, Fe^{2+} binds to FPN1 and triggers a return to the outward-facing open state; and (3) in the extracellular milieu, Fe^{2+} is oxidized to Fe^{3+}, which is taken up by the plasma transferrin and delivered to various tissues throughout the body.(2)

Fundamental questions still remain unanswered about the molecular mechanisms associated with the conformational changes underlying the iron transport cycle, as well as on those ensuring the stability of the outward- and inward-facing conformations. In MFS transporters, a set of specific, so-called “gating” residues, has been suggested to be key actor in interactions between helices from the N- and C-domains that alternately move to form the outward- and inward-facing conformations, as well as a series of intermediate states.(10) Salt bridges and hydrogen bonds are considered particularly important for stabilizing MFS transporters in the outward-facing state. In line with this idea, we recently provided evidence of the formation of a non-covalent, electrostatic interaction between arginine 178 and aspartate 473 on the intracellular side of human FPN1. After also investigating phenotypes related to the recurrent p.Arg178Gln missense mutation, we postulated that the shift of the equilibrium towards the inward-facing state due to a deficient role of gating residues in the intracellular gate could represent a new molecular mechanism of loss of FPN1 function.(15)

Here, using comparative modeling and molecular dynamics (MD) simulations, we predict atomic details for the organization of human FPN1 in the outward-facing open state. *In vitro* evaluation of alanine mutants in different transmembrane helices is interpreted relative to the expected role of the corresponding non-mutated residues in forming non-covalent bonds (salt bridges or hydrogen bonds) between the N-domain and the C-domain of human FPN1. We identified five key residues that play an essential function in the intracellular gate and iron transport cycle. Comparing BbFpn and FPN1 3D structures revealed interactions that may play an important role in the stability of the gate and in the modulation of the conformational changes in the human transporter, some of which cannot be formed in the bacterial homologue. We finally highlight some critical residues that are mutated in patients with a typical hemochromatosis type 4A phenotype.

Material and methods

Modeling and molecular dynamics simulations

As previously reported,(15) a model of the 3D structure of human FPN1 was built using Modeller v9.15(16) considering the sequence alignment reported by Taniguchi et al.(12) and, as template, the experimental 3D structure of *Bdellovibrio bacteriovorus* iron transporter Bd2019 in an outward-facing conformation (pdb 5AYM). Some large regions were discarded from the FPN1 model because no template was available for accurate modeling: amino acids (aa) 1 to 21 (N-terminal sequence), aa 237-301 (linker between the N-domain and the C- domain), and aa 396-450 (TM9-TM10 loop).

A molecular dynamics simulation was run for 100 ns using the human FPN1 3D structure model. This was embedded in a membrane bilayer composed of POPC (2-oleoyl-1-palmitoylsn-glycero-3-phosphocholine) molecules and solvated within a rectangular box of explicit water molecules and 15 mM NaCl. The simulation box (105×105×100 $Å^3$) contained the protein, 275 lipids, 49 Na^+ ions,(19) 53 Cl^- ions,(20) and 18,409 TIP3P water molecules regularly filling the pore and the full box.(21) Minimization, equilibration and production phases/steps used the CHARMM36 force field(18,22) in NAMD 2.9(23) following the protocol described in Hoffmann, Elbahnsi et al., 2018.(24) The RMSDs between the initial model and each snapshot from the MD are given in Supplemental Figure 2. 25 ns appeared sufficient to achieve stable models. Distances between some atoms from critical amino acids along the simulation are provided in Figure 4.

An additional simulation was carried out with 70 mM $CaCl_2$, other parameters being equal, to take account of the role of Ca^{2+} in FPN1-mediated metal efflux. Both simulations (Na^+/Ca^{2+}) were performed in absence of iron, for which the binding site remained to be explored at the experimental level in the outward-facing conformation. The results of the two simulations were quite similar, especially regarding the bond network analyzed here (Supplemental Figure 3). Na^+ ions, however, fluctuated whereas several Ca^{2+} ions were trapped in some regions during simulation, one of them artifactually interacting with a carboxyl group (Lys236) introduced after the truncation of the protein after the N-terminal domain. However, it is worth noting, that overestimated binding affinities of divalent ions are a known problem in classical force fields.(25)

Plasmid constructs

The wild-type FPN1-V5/CD8 bicistronic plasmid construct was generated by cloning full-length human *SLC40A1* and CD8 cDNA (Genbank accession numbers: NM_0414585.5

and NM_001145873.1) into the pIRES2 DsRed-Express2 vector (Clontech); the DsRed-Express2 fluorescent protein coding sequence was removed and replaced by CD8 cDNA, while a V5 epitope tag (GKPIPNPLLGLDST) was introduced in the fifth extracellular loop of FPN1 to facilitate detection on flow cytometry. Iron release measurement used a pcDNA3.1-FPN1-V5(C-ter) construct.(7) All ferroportin mutations were introduced in the pIRES_FPN1-V5_CD8 and pcDNA3.1_FPN-V5 vectors using the QuickChange Site-Directed mutagenesis kit, according to the manufacturer's instructions (Agilent Technologies). Sequencing analyses were performed to check the integrity of all plasmid constructs (full-length *SLC40A1* cDNA sequenced after each site-directed mutagenesis).

Culture and transfection of human epithelial kidney (HEK)293T cells

HEK293T cells, from the American Type Culture Collection, were incubated at 37°C in a 5% CO_2 humidified atmosphere and propagated in Dulbecco's modified Eagle's medium (DMEM, Lonza) supplemented with 10% fetal bovine serum. Cells were transiently transfected using JetPEI (Polyplus), according to the manufacturer's instructions, and a 2:1 transfection reagent (µL)/plasmid DNA ratio (µg).

Flow cytometry

HEK293T cells (1.9 x 10^5 cells per well in 12-well plates) transfected with the pIRES_FPN1-V5_CD8 constructs were harvested with trypsin 36h post-transfection. Samples were pelleted (500 x g, 5 min) and resuspended in Phosphate-Buffered Saline (PBS, pH 7.4) containing 1 mM EDTA and 10% Fetal Bovine Serum (FBS), before being incubated for 30 min at 4°C with anti-V5-FITC (Thermo Fisher Scientific) and anti-CD8-APC (Miltenyi Biotec). Stained cells were pelleted (500 x g, 5 min, 4°C) and resuspended in 400 µL PBS-EDTA. Cells were analyzed using a BD Accuri C6 flow cytometer (Becton Dickinson) and Flowlogic™ software (Miltenyi Biotec). Events were gated to: i) exclude cell debris and aggregates, and ii) select cells with the desired levels of CD8 and FPN1-V5 expression; the windows were set up to exclude CD8- or FPN1-V5-negative cells (using mock-transfected cells as control), as well as cells with very high fluorescent intensity.

Intracellular ^{55}Fe measurements

^{55}Fe loading of human apotransferrin was performed as previously described.(26) HEK293T cells (1.7 x 10^5cells per well in 12-well plates) were transfected with wild-type or mutated pcDNA3.1_FPN-V5 constructs for 24h, before being cultured in Pro293a-CDM serum-free medium (Biowhittaker) and preloaded with 20 µg/mL ^{55}Fe-transferrin for 16h.

Each pcDNA3.1_FPN-V5 construct was co-delivered with the pSV-β-Galactosidase vector (Promega). Cells were harvested with trypsin, mixed with liquid scintillation fluid (Ultima Gold MV, Perkin Elmer) and counted for 2 min in a TRI-CARB 1600 CA scintillation counter (Perkin Elmer). ^{55}Fe radioactivity was normalized on total protein content and β-GAL activity.

Statistical analysis

Data are presented as mean (column bars) with standard deviation. Comparisons used two-tailed Student t-test.

Results

Model of the 3D structure of the outward-facing conformation of human ferroportin 1

As previously reported,(15) a model of the 3D structure of human ferroportin 1 in an outward-facing conformation was built using the BbFpn structure (Bd2019; pdb 5AYM) as template (see Material and Methods). On the intracellular side (cytoplasmic gate), TM2, TM3, TM4 and TM5 (N-domain) interact tightly with TM10 and TM11 (C-domain) (Figure 1A). Human ferroportin 1 conserves the amino acid atoms thought to play a critical role in the BbFpn cytoplasmic gate.(12) Asp157 (TM4, *BbFpn Asp140*) forms salt-bridges with Arg88 (TM3, *BbFpn Arg73*) and Arg489 (TM11, *BbFpn Arg371*), whereas Arg88 also forms a salt-bridge with Glu486 (preceding TM11, *BbFpn Glu368*) (Figure 1A, green box at right). This network is completed with that provided by H-bonds formed, on the one hand, between the side chain oxygens of Asp84 (TM2, *BbFpn Asp69*) and the main chain nitrogen atoms of Gly490 and Ile491 (TM11) (*BbFpn Gly372 and Glu373*) (Figure 1A, green box at right) and, on the other hand, between the sides chains of Asn174 (TM5, *BbFpn Asn155*) and Gln481 (TM10, *BbFpn Gln363*) (Figure 1A, orange box at left). The previously reported salt-bridge between Arg178 and Asp473 also participates in this network.(15)

A simplified view of the inter-domain and intra-domain interactions for both the bacterial and the human iron exporter is provided in Supplementary Figure 1.

In-vitro evaluation of seven candidate gating residues

To experimentally test the 3D model for the intracellular gate, we individually mutagenized arginine 88, aspartic acid 157, glutamic acid 486, arginine 489, aspartic acid 84 and glutamine 481 to alanine. Alanine is the second smallest amino acid after glycine. This

non-polar amino acid has the highest propensity of all 20 natural amino acids for the alpha-helical state.(27) The selected alanine substitutions were thus likely to have limited impact on local human ferroportin 1 structure. Only asparagine 174 was mutated to isoleucine, as the p.Asn174Ile missense mutation was previously proved to be defective for iron egress while being normally addressed to the cell surface.(7,28)

A bicistronic construct was used to evaluate the concurrent plasma membrane expression of human ferroportin 1 (conjugated with a V5 epitope) and cluster of differentiation 8 (CD8) on flow cytometry. Taking account of the level of CD8 in HEK293T cells, which do not normally express this membrane protein, enabled correction for differences in transfection efficiency between samples. The p.Ala77Asp missense mutation, which significantly damages ferroportin 1 structure and is known to prevent cell-surface localization, was used as negative control. It was noteworthy that expression of FPN1-V5 fusion proteins was lower than the CD8 control in all analyzed cell populations (cells expressing wild-type FPN1-V5 fusion displayed >40% reduction); this suggests differences in the levels of FPN1 and CD8 translation initiated from the bicistronic mRNA. An important difference was observed in the proportions of FPN1-WT+/CD8+ and FPN1-A77D+/CD8 cells ($p<0.001$), confirming that the p.Ala77Asp mutant causes ferroportin 1 mislocalization (Figure 2A). Expression of the p.Asp84Ala mutant also differed significantly from the wild-type protein ($p<0.05$). The other six variants reached the plasma membrane correctly.

Radioactively labeled iron accumulation was measured in HEK293T cells transiently transfected with pcDNA3.1 plasmids encoding FPN1-V5 fusion proteins, using cells transfected with the commercial pcDNA3.1-V5-His empty vector as control. pcDNA3.1 plasmids were co-delivered with a normalization vector encoding the β-galactosidase enzyme. Twenty-four hours after transfection, HEK293T cells were cultured in serum-free medium and pre-loaded with 20 µg/mL ^{55}Fe-transferrin for 16h. The cell lysates were assayed for ^{55}Fe quantity, β-GAL activity (to correct for differences in transfection efficiency) and total protein concentration (to correct for differences in final cell number). As shown in Figure 2B, cells transfected with the wild-type FPN1-V5 fusion protein displayed 2- to 3- fold lower iron accumulation. The p.Arg88Ala, p.Asp157Ala, p.Arg489Ala, p.Asp84Ala and p.Asn174Ile mutants were not able to export ^{55}Fe iron in amounts comparable with wild-type FPN1. Two mutants, p.Gln481Ala and p.Glu486Ala, retained their ability to export iron out of the cell.

Taken together, the results shown in Figure 2 A-B demonstrate that arginine 88, aspartic acid 157, arginine 489 and asparagine 174 are important for iron export. In contrast, glutamine 481 and glutamic acid 486 can be changed to alanine without altering FPN1 function. In the light of this, we then investigated the function of the p.Gln481Ala-Glu486Ala double mutant. Figure 3 A-B shows that it localized to the cell surface in the same way as the wild-type protein and that it retained export function.

Molecular Dynamics (MD) simulations

To further understand the differences observed for the mutants tested, molecular dynamics simulations were run on the human FPN1 3D structure model in an appropriate environment (Material and Methods). Root mean square deviations (RMSD) for the protein backbone during 100 ns MD simulation were calculated relative to the coordinates of the initial structures (Supplemental Figure 2). More constant values were observed from 20-25 ns onwards, after an initial 10-ns fast-rise region, indicating that the model structure had reached conformation steady state.

Comparing conformations in this steady state (illustrated here at 100 ns; Figure 1B) to the initial 3D structure (0 ns; Figure 1A) revealed a slight reorganization of the intracellular gate bond network. While the salt-bridges between Asp157 and Arg88 and Asp157 and Arg489 appeared very stable throughout the simulation, as assessed by monitoring the distances between the involved atoms (Figure 4A), Glu486 moved away, with its two side-chain oxygen atoms usually free from any interaction. Interestingly, the two H-bonds between Asp84 and the main-chain N atoms of Gly490 and Ile491 were rapidly lost and only occasionally reformed (Figure 4B), while one of the side-chain oxygen atoms of Asp84 was able to form a salt-bridge with Lys85, itself bound to Asp81 (Figure 4C). This double salt-bridge was not constant throughout the simulation, with variable positions of Lys85 side chain and transient H-bonds of Asp84 with Gly490 and Ile491 main-chain N atoms, suggesting that this feature may be a key-point for conformational change during the human FPN1 cycle. It was noteworthy that these bonds could not be formed in the BbFpn structure, as the amino acids homologous to Asp81 and Lys85 are Lys66 and Thr70, respectively. Finally, the H bond between Gln481 and Asn174 was also not maintained, and occurred very rarely during the simulation (Figure 4D). In contrast, Asn174 made other H-bonds with Gln478 on TM10 and Arg178 on TM5, Arg178 also forming an inter-lobe salt-bridge with Asp473, as previously reported.(15)

In conclusion, these results explain the non-critical role of Gln481 and Glu486 for the FPN1 function, highlight an alternative functional role of Asp84 in a dynamic network

and suggest a critical role for Gln478, interacting with Asn174, itself included in a wide bond network involving Arg178 and Asp473. These three features were not anticipated from the experimental static 3D structure of BbFpn.

In-vitro evaluation of the Gln478Ala mutant

To check our predictions, we also evaluated the effects of the Gln478Ala mutant. The mutant was detected on the surface of HEK293T transiently transfected cells at levels similar to those seen with the wild type protein (Figure 5A). Its ability to export iron out the cell was, however, markedly reduced (Figure 5B). Of note, functional consequences of the Gln478Ala mutant were comparable to those observed for the Asn174Ile mutant (Figures 2 A-B).

Genotype-phenotype correlations

Based on the literature, we identified 13 missense mutations that affect 7 different gating residues (Asp84, Arg88, Asp157, Asn174, Arg178, Arg489 and Gly490) and have been reported in a total of 77 patients (32 female, 45 male; Table 1). As summarized in Figure 6, most patients presented serum ferritin >1000 µg/L and transferrin saturation <50% (females) or <60% (males) at diagnosis. This is characteristic of the hemochromatosis type 4A subtype and FPN1 loss-of-function.(29,30)

Discussion

In-depth knowledge of the main elements of normal ferroportin 1 physiology is an important prerequisite for understanding the mechanism of iron export in mammals. Here, we investigated the structure-function relationships of a set of amino acids previously predicted, from the bacterial homologue BbFpn 3D structure, as key elements for stabilizing the protein in the outward-facing state. This revealed non-covalent interactions between several amino acids that are conserved between species and form a first essential interaction network. Moreover, molecular dynamic simulations performed on the model of the human FPN1 3D structure led to explain the non-critical role of a few amino acids and to reveal other critical ones, which were further supported at the experimental level. These additional residues are also permanently involved in non-covalent interactions, with either a unique or multiple partners, within networks that are specific to human FPN1. This study thus provides for the first time an accurate topological description of the human FPN1 intracellular gate.

MFS transporters must undergo large conformational changes to transport substrates across membranes through alternate access mechanism. Accordingly, gates are found at each end of the protein, which open and lock in concert to allow passage of substrates. Gating residues comprise amino acids that mediate interactions between the N- and C- domains in one conformational state. Such contacts are important not only for stabilizing the different conformational states but also for ensuring cooperation in conformational changes, preventing forbidden states with both gates open.(10) Gating residues in MFS proteins often involve charged residues forming salt-bridges,(31,32) but this appears to be a recurrent feature of several membrane systems.(33) Salt-bridges can also be found in the central cavities of membrane domains, stabilizing specific conformations.(24,34) The 3D structure of BbFpn suggests that the intra- and extracellular gates clearly differ, involving salt-bridge/H-bonds and hydrophobic contacts, respectively.(12)

Investigating both the 3D structure of human FPN1 and the cellular effects of alanine-substituted mutants (Figures 1 and 2) confirmed the existence of salt-bridges between Arg88 (TM3), Asp157 (TM4) and Arg489 (TM11). These electrostatic interactions, involving conserved residues and appearing very stable along molecular dynamic simulations (supplemental Figure 3A), are completed by another inter-domain salt-bridge between Arg178 (TM5) and Asp473 (TM10), as we demonstrated very recently.(15) Interestingly, this last salt-bridge appears specific to human FNP1; it can not exist in the BbFpn structure as the residue equivalent to Asp473 is Ser355. The whole salt-bridge network described here is likely very important for stabilization of human FPN1 in the outward-open conformation.

An intriguing issue was the observation that Gln481 (TM10) and Glu486 (preceding TM11), which were predicted from the BpFpn structure (corresponding amino acids Gln363 and Glu368) as also involved in the intracellular gate, are not essential to human FPN1 activity. These observations were reinforced by the study of the Gln481Ala-Glu486Ala double mutant, which was indistinguishable from the wild-type protein for cell-surface expression and iron export ability (Figure 3). This marks a clear difference from hypotheses based on the bacterial homologue outward-facing structure, and this can only be explained after molecular dynamics simulations and refinement of the model of the 3D structure of human FPN1. Hence, Gln481 is thought to interact only transiently with Asn174 (TM5), which actually forms quasi-stable H-bonds with both Gln478 (TM10) and Arg178 (TM5) (Figures 1 and 4). The two side-chain oxygen atoms in Glu486 are very often free of any interaction (Figure 1 and Figure 4A), and Glu486 is thus unable to

actively participate in the interaction network formed by Arg88, Asp157 and Arg489. The situation of Asp84 is even more complex, since it relies on local interactions that do not exist in the bacterial homologue BbFpn. Indeed, Asp84 is expected to briefly form H-bonds with both the main chain N atoms of Gly490 and Ile491, when not forming a salt-bridge with Lys85. The local network involving Asp84 and Lys85 in TM2 can be reinforced by an additional bond between Lys85 and Asp81 (Figure 1 and Figures 4B-C-D). Important conclusions to our study, supported at the experimental level, are thus the identification of Gln478 as an additional critical actor of the human FPN1 intracellular gate, and of the involvement of Asn174 and Asp84 in multiple bonds also playing a fundamental role in this gate. Interestingly, these networks of interactions involve residues that are specific to human FPN1: Asp473, Gln478, Asp81 and Lys85 (Ser355, Glu360, Lys66 and Thr70, respectively, in BbFpn).

Worth noting is the potential role that surrounding phospholipids may play in the structural rearrangements enabling alternate access mechanism, by interfering with the conserved network of interactions in the cytoplasmic gate. In particular, phosphatidylethanolamine lipids may directly interact with some acidic residues of the intracellular gate charged network, such as Asp84, and stabilize the inward-facing conformation by interfering with contacts between the cytoplasmic ends of the N- and C-lobe. The role of such molecular switches in the dynamic interconversion underpinning transport cycle has been described for some other MFS transporters;(35,36) it should be further investigated in the particular case of ferroportin 1.

Like other adult-onset autosomal dominant diseases, hemochromatosis type 4A (or ferroportin disease) is characterized by incomplete penetrance and wide phenotypic heterogeneity. Thus far, 51 missense mutations have been associated with the disease.(29,37,38) Not all have been functionally investigated, and not all have been definitively identified as disease-causing. It is, however, interesting that 13 missense mutations map to the FPN1 intracellular gate. They correspond to 7 gating residues (Asp84, Arg88, Asp157, Asn174, Arg178 Arg489 and Gly490) that, according our investigations, are involved in the formation of non-covalent interactions at the interface between the N- and the C-domains (Figure 1). As illustrated in Figure 6, patients with these missense mutations generally present high serum ferritin concentrations (>1000 µg/L), suggesting significant iron overload in tissue, related to serious FPN1 dysfunction. The ~~p.Asp84Glu,~~ p.Asp157Gly, p.Asp157Tyr and p.Arg489Lys substitutions are known to cause FPN1 mislocalization.(39,40) This likely results from folding defects in transmembrane helices 2, 4 or 11 and/or local unstability of the structure. By contrast, the

p.Arg88Gly, p.Asp157Ala, p.Asn174Ile and p.Arg178Gln substitutions reduce the ability of FPN1 to export iron without defective cell surface expression.(7,15,28) This is now explained by the loss of inter-domain interactions in the outwardly-oriented FPN1 state. The p.Arg88Thr, p.Asp157Asn and p.Arg489Ser substitutions have not yet been studied experimentally; in the light of above observations, however, it can reasonably be anticipated that they are all deleterious.

To conclude, the present study provides an unprecedented view of the interactions needed to form and stabilize the FPN1 intracellular gate. It highlights intra- and inter-domain interactions, some of which not existing in the bacterial homologue BbFpn, thus identifying the fundamental role of a set of specific residues in the iron transport cycle in humans. It also confirms that hemochromatosis type 4A is not restricted to missense mutations that cause protein mislocalization, thus increasing our ability to interpret rare genetic variants at the *SLC40A1* locus. This will have profound implications for patient management. More extensive molecular dynamics simulations are warranted, to understand the mechanisms associated with the conformational changes leading to the inward-facing conformation and the influence of iron and calcium binding and release. Particular attention should also be paid to the identification of hydrophobic inter-domain interactions in the inward-facing structure of FPN1. This is necessary in order to identify all the network of gating residues that participate in the global transition from the outward-facing to the inward-facing state and vice versa. (37,41–54)

References

1. Anderson GJ, Frazer DM. Current understanding of iron homeostasis. Am J Clin Nutr. 2017 Dec;106(Suppl 6):1559S-1566S.

2. Drakesmith H, Nemeth E, Ganz T. Ironing out Ferroportin. Cell Metab. 2015 Nov 3;22(5):777–87.

3. Hentze MW, Muckenthaler MU, Galy B, Camaschella C. Two to tango: regulation of Mammalian iron metabolism. Cell. 2010 Jul 9;142(1):24–38.

4. Donovan A, Lima CA, Pinkus JL, Pinkus GS, Zon LI, Robine S, et al. The iron exporter ferroportin/Slc40a1 is essential for iron homeostasis. Cell Metab. 2005 Mar;1(3):191–200.

5. Nemeth E, Tuttle MS, Powelson J, Vaughn MB, Donovan A, Ward DM, et al. Hepcidin regulates cellular iron efflux by binding to ferroportin and inducing its internalization. Science. 2004 Dec 17;306(5704):2090–3.

6. Girelli D, Nemeth E, Swinkels DW. Hepcidin in the diagnosis of iron disorders. Blood. 2016 Jun 9;127(23):2809–13.

7. Le Gac G, Ka C, Joubrel R, Gourlaouen I, Lehn P, Mornon J-P, et al. Structure-function analysis of the human ferroportin iron exporter (SLC40A1): effect of hemochromatosis type 4 disease mutations and identification of critical residues. Hum Mutat. 2013 Oct;34(10):1371–80.

8. Wallace DF, Harris JM, Subramaniam VN. Functional analysis and theoretical modeling of ferroportin reveals clustering of mutations according to phenotype. Am J Physiol Cell Physiol. 2010 Jan;298(1):C75-84.

9. Bonaccorsi di Patti MC, Polticelli F, Cece G, Cutone A, Felici F, Persichini T, et al. A structural model of human ferroportin and of its iron binding site. FEBS J. 2014 Jun;281(12):2851–60.

10. Quistgaard EM, Löw C, Guettou F, Nordlund P. Understanding transport by the major facilitator superfamily (MFS): structures pave the way. Nat Rev Mol Cell Biol. 2016;17(2):123–32.

11. Bonaccorsi di Patti MC, Polticelli F, Tortosa V, Furbetta PA, Musci G. A bacterial homologue of the human iron exporter ferroportin. FEBS Lett. 2015 Dec 21;589(24 Pt B):3829–35.

12. Taniguchi R, Kato HE, Font J, Deshpande CN, Wada M, Ito K, et al. Outward- and inward-facing structures of a putative bacterial transition-metal transporter with homology to ferroportin. Nat Commun. 2015 Oct 13;6:8545.

13. Deshpande CN, Ruwe TA, Shawki A, Xin V, Vieth KR, Valore EV, et al. Calcium is an essential cofactor for metal efflux by the ferroportin transporter family. Nat Commun. 2018 Aug 6;9(1):3075.

14. Jardetzky O. Simple allosteric model for membrane pumps. Nature. 1966 Aug 27;211(5052):969–70.

15. Ka C, Guellec J, Pepermans X, Kannengiesser C, Ged C, Wuyts W, et al. The SLC40A1 R178Q mutation is a recurrent cause of hemochromatosis and is associated with a novel pathogenic mechanism. Haematologica. 2018 Nov;103(11):1796–805.

16. Webb B, Sali A. Protein Structure Modeling with MODELLER. Methods Mol Biol Clifton NJ. 2017;1654:39–54.

17. Hoffmann B, Elbahnsi A, Lehn P, Décout J-L, Pietrucci F, Mornon J-P, et al. Combining theoretical and experimental data to decipher CFTR 3D structures and functions. Cell Mol Life Sci CMLS. 2018 Oct;75(20):3829–55.

18. Jo S, Cheng X, Lee J, Kim S, Park S-J, Patel DS, et al. CHARMM-GUI 10 years for biomolecular modeling and simulation. J Comput Chem. 2017 Jun 5;38(15):1114–24.

19. Lamoureux G, Roux B. Absolute hydration free energy scale for alkali and halide ions established from simulations with a polarizable force field. J Phys Chem B. 2006 Feb 23;110(7):3308–22.

20. Beglov D, Roux B. Finite representation of an infinite bulk system: Solvent boundary potential for computer simulations. J Chem Phys. 1994 Jun 15;100(12):9050–63.

21. Jorgensen WL, Chandrasekhar J, Madura JD, Impey RW, Klein ML. Comparison of simple potential functions for simulating liquid water. J Chem Phys. 1983 Jul 15;79(2):926–35.

22. Hart K, Foloppe N, Baker CM, Denning EJ, Nilsson L, Mackerell AD. Optimization of the CHARMM additive force field for DNA: Improved treatment of the BI/BII conformational equilibrium. J Chem Theory Comput. 2012 Jan 10;8(1):348–62.

23. Phillips JC, Braun R, Wang W, Gumbart J, Tajkhorshid E, Villa E, et al. Scalable molecular dynamics with NAMD. J Comput Chem. 2005 Dec;26(16):1781–802.

24. Hoffmann B, Elbahnsi A, Lehn P, Décout J-L, Pietrucci F, Mornon J-P, et al. Combining theoretical and experimental data to decipher CFTR 3D structures and functions. Cell Mol Life Sci CMLS. 2018 Oct;75(20):3829–55.

25. Heinz LP, Kopec W, de Groot BL, Fink RHA. In silico assessment of the conduction mechanism of the Ryanodine Receptor 1 reveals previously unknown exit pathways. Sci Rep. 2018 May 2;8(1):6886.

26. Ka C, Le Gac G, Dupradeau F-Y, Rochette J, Férec C. The Q283P amino-acid change in HFE leads to structural and functional consequences similar to those described for the mutated 282Y HFE protein. Hum Genet. 2005 Sep;117(5):467–75.

27. Callebaut I, Labesse G, Durand P, Poupon A, Canard L, Chomilier J, et al. Deciphering protein sequence information through hydrophobic cluster analysis (HCA): current status and perspectives. Cell Mol Life Sci CMLS. 1997 Aug;53(8):621–45.

28. De Domenico I, McVey Ward D, Nemeth E, Ganz T, Corradini E, Ferrara F, et al. Molecular and clinical correlates in iron overload associated with mutations in ferroportin. Haematologica. 2006 Aug;91(8):1092–5.

29. Pietrangelo A. Ferroportin disease: pathogenesis, diagnosis and treatment. Haematologica. 2017 Dec;102(12):1972–84.

30. Vlasveld LT, Swinkels DW. Loss-of-function ferroportin disease: novel mechanistic insights and unanswered questions. Haematologica. 2018 Nov;103(11):1753–5.

31. Fowler PW, Orwick-Rydmark M, Radestock S, Solcan N, Dijkman PM, Lyons JA, et al. Gating topology of the proton-coupled oligopeptide symporters. Struct Lond Engl 1993. 2015 Feb 3;23(2):290–301.

32. Solcan N, Kwok J, Fowler PW, Cameron AD, Drew D, Iwata S, et al. Alternating access mechanism in the POT family of oligopeptide transporters. EMBO J. 2012 Aug 15;31(16):3411–21.

33. Latorraca NR, Fastman NM, Venkatakrishnan AJ, Frommer WB, Dror RO, Feng L. Mechanism of Substrate Translocation in an Alternating Access Transporter. Cell. 2017 23;169(1):96-107.e12.

34. Stelzl LS, Fowler PW, Sansom MSP, Beckstein O. Flexible gates generate occluded intermediates in the transport cycle of LacY. J Mol Biol. 2014 Feb 6;426(3):735–51.

35. Martens C, Shekhar M, Borysik AJ, Lau AM, Reading E, Tajkhorshid E, et al. Direct protein-lipid interactions shape the conformational landscape of secondary transporters. Nat Commun. 2018 08;9(1):4151.

36. Corradi V, Sejdiu BI, Mesa-Galloso H, Abdizadeh H, Noskov SY, Marrink SJ, et al. Emerging Diversity in Lipid-Protein Interactions. Chem Rev. 2019 May 8;119(9):5775–848.

37. Majore S, Bonaccorsi di Patti MC, Valiante M, Polticelli F, Cortese A, Di Bartolomeo S, et al. Characterization of three novel pathogenic SLC40A1 mutations and genotype/phenotype correlations in 7 Italian families with type 4 hereditary hemochromatosis. Biochim Biophys Acta Mol Basis Dis. 2018 Feb;1864(2):464–70.

38. Wang Y, Du Y, Liu G, Guo S, Hou B, Jiang X, et al. Identification of novel mutations in HFE, HFE2, TfR2, and SLC40A1 genes in Chinese patients affected by hereditary hemochromatosis. Int J Hematol. 2017 Apr;105(4):521–5.

39. Callebaut I, Joubrel R, Pissard S, Kannengiesser C, Gérolami V, Ged C, et al. Comprehensive functional annotation of 18 missense mutations found in suspected hemochromatosis type 4 patients. Hum Mol Genet. 2014 Sep 1;23(17):4479–90.

40. Griffiths WJH, Mayr R, McFarlane I, Hermann M, Halsall DJ, Zoller H, et al. Clinical presentation and molecular pathophysiology of autosomal dominant hemochromatosis caused by a novel ferroportin mutation. Hepatol Baltim Md. 2010 Mar;51(3):788–95.

41. Wallace DF, McDonald CJ, Ostini L, Iser D, Tuckfield A, Subramaniam VN. The dynamics of hepcidin-ferroportin internalization and consequences of a novel ferroportin disease mutation. Am J Hematol. 2017 Oct;92(10):1052–61.

42. Bach V, Remacha A, Altés A, Barceló MJ, Molina MA, Baiget M. Autosomal dominant hereditary hemochromatosis associated with two novel Ferroportin 1 mutations in Spain. Blood Cells Mol Dis. 2006 Feb;36(1):41–5.

43. Cunat S, Giansily-Blaizot M, Bismuth M, Blanc F, Dereure O, Larrey D, et al. Global sequencing approach for characterizing the molecular background of hereditary iron disorders. Clin Chem. 2007 Dec;53(12):2060–9.

44. Saja K, Bignell P, Robson K, Provan D. A novel missense mutation c.470 A>C (p.D157A) in the SLC40A1 gene as a cause of ferroportin disease in a family with hyperferritinaemia. Br J Haematol. 2010 Jun;149(6):914–6.

45. Muehlenberg K, Faltermeier N, Lohse P, Tannapfel A, Pech O. [Family with marked hyperferritinemia as a result of hemochromatosis type 4 (ferroportin disease)]. Z Gastroenterol. 2014 Sep;52(9):1075–80.

46. Hattori A, Miyajima H, Tomosugi N, Tatsumi Y, Hayashi H, Wakusawa S. Clinicopathological study of Japanese patients with genetic iron overload syndromes. Pathol Int. 2012 Sep;62(9):612–8.

47. Yamashita T, Morotomi N, Sohda T, Hayashi H, Yoshida N, Ochi K, et al. A male patient with ferroportin disease B and a female patient with iron overload similar to ferroportin disease B. Clin J Gastroenterol. 2014 Jun;7(3):260–4.

48. Hetet G, Devaux I, Soufir N, Grandchamp B, Beaumont C. Molecular analyses of patients with hyperferritinemia and normal serum iron values reveal both L ferritin IRE and 3 new ferroportin (slc11A3) mutations. Blood. 2003 Sep 1;102(5):1904–10.

49. Kaneko Y, Miyajima H, Piperno A, Tomosugi N, Hayashi H, Morotomi N, et al. Measurement of serum hepcidin-25 levels as a potential test for diagnosing hemochromatosis and related disorders. J Gastroenterol. 2010 Nov;45(11):1163–71.

50. Pelucchi S, Mariani R, Salvioni A, Bonfadini S, Riva A, Bertola F, et al. Novel mutations of the ferroportin gene (SLC40A1): analysis of 56 consecutive patients with unexplained iron overload. Clin Genet. 2008 Feb;73(2):171–8.

51. Corradini E, Montosi G, Ferrara F, Caleffi A, Pignatti E, Barelli S, et al. Lack of enterocyte iron accumulation in the ferroportin disease. Blood Cells Mol Dis. 2005 Dec;35(3):315–8.

52. Speletas M, Kioumi A, Loules G, Hytiroglou P, Tsitouridis J, Christakis J, et al. Analysis of SLC40A1 gene at the mRNA level reveals rapidly the causative mutations in patients with hereditary hemochromatosis type IV. Blood Cells Mol Dis. 2008 Jun;40(3):353–9.

53. Koyama C, Wakusawa S, Hayashi H, Ueno T, Suzuki R, Yano M, et al. A Japanese family with ferroportin disease caused by a novel mutation of SLC40A1 gene: hyperferritinemia associated with a relatively low transferrin saturation of iron. Intern Med Tokyo Jpn. 2005 Sep;44(9):990–3.

54. Jouanolle A-M, Douabin-Gicquel V, Halimi C, Loréal O, Fergelot P, Delacour T, et al. Novel mutation in ferroportin 1 gene is associated with autosomal dominant iron overload. J Hepatol. 2003 Aug;39(2):286–9.

55. Pettersen EF, Goddard TD, Huang CC, Couch GS, Greenblatt DM, Meng EC, et al. UCSF Chimera--a visualization system for exploratory research and analysis. J Comput Chem. 2004 Oct;25(13):1605–12.

Acknowledgments

The protocol used for molecular dynamics simulation was developed during our research work on the CFTR protein, which was supported by the French Association “Vaincre La Mucoviscidose” and performed using HPC resources from GENCI-[CINES] (Grant 2017-A0020707206, 2018-A0040707206 and 2019-A0060707206). This work was also supported by grants from the French Hospital Clinical Research Program (Progamme Hospitalier de Recherche Clinique 2009; Brest University Hospital UF0857), the Gaetan Saleun Association and the GR-Ex Laboratory of Excellence (reference ANR-11-LABX-0051). The labex GR-Ex is funded by the IdEx program “Investissements d’avenir” of the French National Research Agency (reference ANR-18-IDEX-0001). We thank George Gao and Alain R.M. Townsend for generous gift of the CD8 expression vector.

Authorship contributions

G. Le Gac and I. Callebaut designed the study. I. Callebaut, A. Elbahnsi, J. Guellec, M. Le Tertre, K. Uguen and I. Gourlaouen conducted experiments. G. Le Gac, I. Callebaut, C. Ka and C. Férec analyzed data. G. Le Gac and I. Callebaut wrote the manuscript. All authors contributed to the editing of the final manuscript.

Figure 1. Model of the 3D structure of the human ferroportin 1 cytoplasmic gate

(A) before (0 ns) and (B) after (100ns) MD simulation.

The 3D structure is shown in a ribbon representation, with amino acids involved in salt-bridges or H-bonds depicted in a ball-and-stick representation. Transmembrane helices (TM) are labeled and colored (TM1-TM3: blue, TM4-TM6: green, TM7-TM9: yellow, TM10-TM12: red). This figure was drawn using Chimera. For convenience, amino acids are described by a one-letter code, instead of the three-letter code used in the main text.

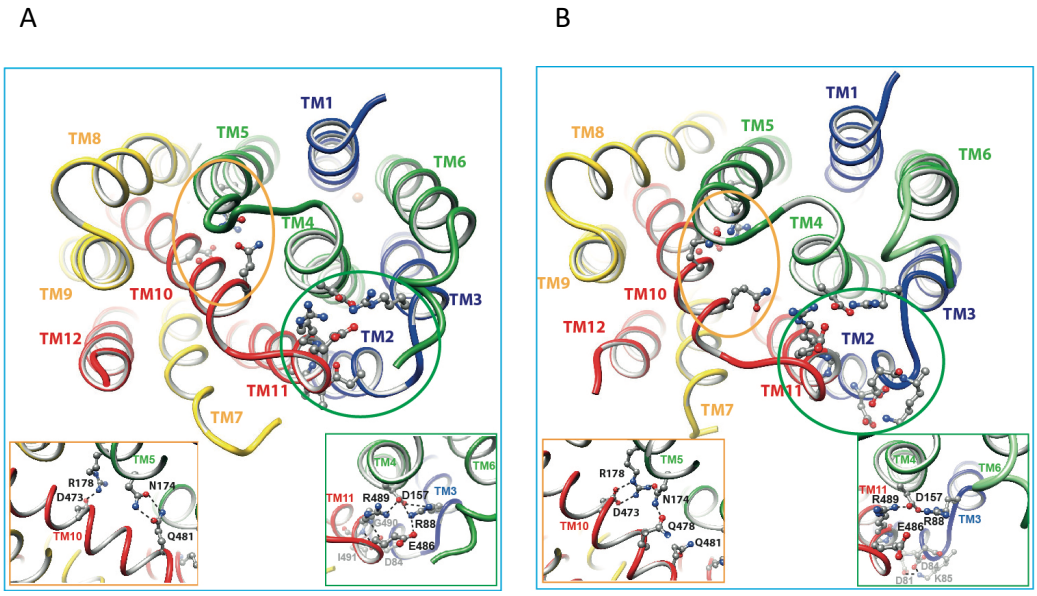

Figure 2. Effect on cell-surface expression and iron export of alanine or isoleucine substitutions for amino acids predicted to be involved in interactions between the N- and the C-lobe of human ferroportin 1 in the outward-facing state.

Green bars indicate residues predicted to form salt-bridges or hydrogen bonds between helices 2, 3, 4 and 11. Orange bars indicate residues predicted to form a hydrogen bond between helices 5 and 10. For convenience, amino acids are described by a one-letter code, instead of the three-letter code used in the main text.

(A) HEK293T cells were transiently transfected with the bicistronic pIRES2 plasmid encoding both full-length human ferroportin 1 and the cluster of differentiation antigen 8 (CD8). A 14-amino-acid V5 epitope (Gly-Lys-Pro-Ile-Pro-Asn-Pro-Leu-Leu-Gly-Leu-Asp-Ser-Thr) was inserted in the fifth extracellular loop (ES5) of FPN1 to allow plasma membrane detection. After 36h, cells were double-stained for CD8 (APC) and the FPN1-V5 fusion protein (FITC) and analyzed by 2-color flow cytometry. Data are presented as percentage of FPN1-positive over CD8-positive events. Each bar represents the mean ± standard deviation of 6 independent experiments. P values were calculated on Student t-test; **P*<0.05 and ****P*<0.001. (B) HEK293T cells were transfected with pcDNA3.1-FPN1-V5-His vectors, grown for 24h00, and then fed with 20 μg/mL ^{55}Fe-transferrin for 16h. Cells were then washed, and counted. Counts per minute (cpm) were normalized by total protein and β–Gal activity. Empty vector (No FPN) samples taken as 100% values generally achieved 1,000 – 2,500 cpm. Each bar represents the mean ± standard deviation of 5 independent experiments. P values were calculated on Student t-test; **P*<0.05 and ***P*<0.01 compared with wild type FPN1.

A

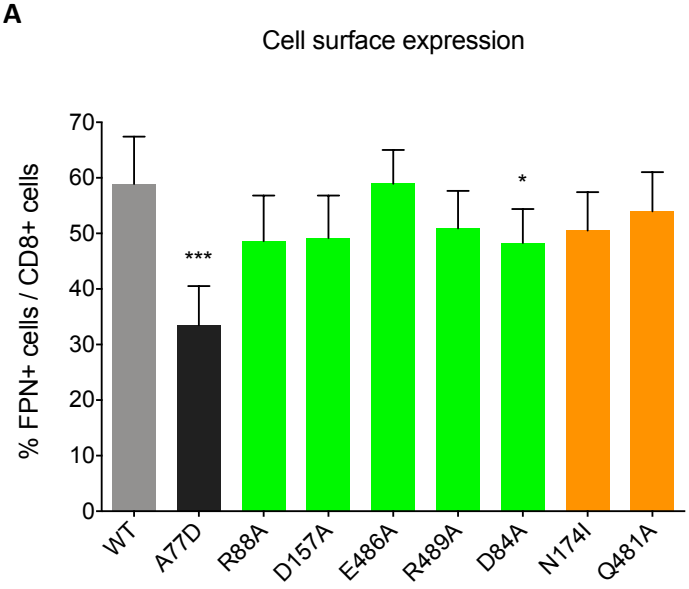
Cell surface expression
% FPN+ cells / CD8+ cells
70
60
50
40
30
20
10
0
***
*
WT
A77D
R88A
D157A
E486A
R489A
D84A
N174I
Q481A

B

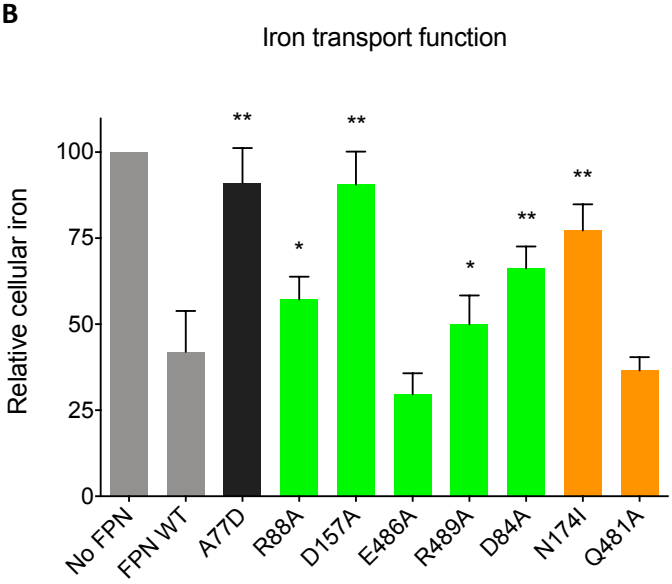
Iron transport function
Relative cellular iron
100
75
50
25
0
**
**
*
*
**
**
No FPN
FPN WT
A77D
R88A
D157A
E486A
R489A
D84A
N174I
Q481A

Figure 3. Cell-surface expression and iron export ability of the Gln481Ala/Glu486Ala double mutant.

(A) HEK293T cells were transiently transfected with the bicistronic pIRES2 plasmid encoding both full-length human ferroportin 1 and the cluster of differentiation antigen 8 (CD8). After 36h, cells were double-stained for CD8 (APC) and the FPN1-V5 fusion protein (FITC) and analyzed by 2-color flow cytometry. Data are presented as percentage of FPN1-positive over CD8-positive events. Each bar represents the mean ± standard deviation of 4 independent experiments. (B) HEK293T cells were transfected with pcDNA3.1-FPN1-V5-His vectors, grown for 24h00, and then fed with 20μg/mL of ^{55}Fe-transferrin for 16h. Cells were then washed and counted. Counts per minute (cpm) were normalized by total protein and β–Gal activity. Each bar represents the mean ± standard deviation of 5 independent experiments.

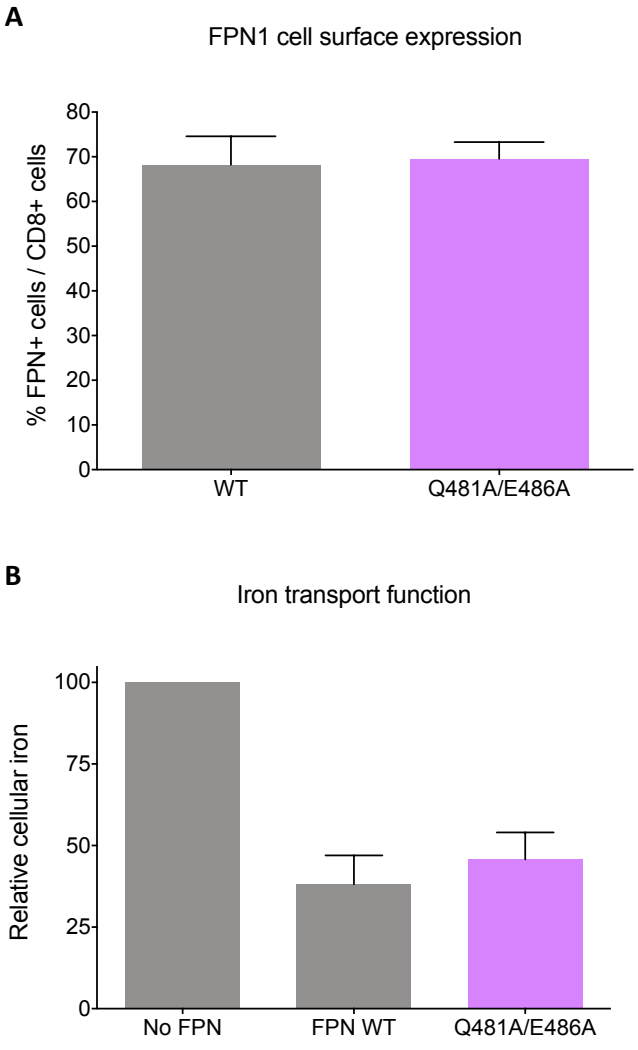

Figure 4. Evolution, along the MD simulation, of the distances between atoms involved in non-covalent bonds. Distances were plotted (using gnuplot) as a function of trajectory time between pairs of atoms (N, OD1, OD2, OE1, OE2, ND2, NE1, NH1, NH2, NZ), which may be involved in non-covalent bonds and are reported here considering the groups depicted in Figure 1. The distance of 5 Å (horizontal grey line) is indicated as a reference, below which bonds can be observed.

Green box of Figure 1 : A) inter-helical side chain-side chain interactions involving TM3 (ARG88), TM4 (ASP157) and TM11 (GLU486, ARG489); B) inter-helical side chain-main chain interactions involving oxygen atoms (OD1/OD2) of the side chain of ASP84 and the nitrogen main chain atom (N) of GLY490 and ILE491; C) intra-helical side chain-side chain interactions at the level of TM2 involving ASP84, LYS85, ASP88 and ARG88. At right are represented three different conformational states extracted from the simulation, illustrating different positions of the side chains of GLU486 and LYS85.

Orange box of Figure 1 : D) inter-helical side chain-side chain interactions involving TM5 (ASN174) and TM10 (GLN478 and GLN481).

The inset between panels C and D represents three different conformational states extracted from the simulation, illustrating different positions of the side chains of Glu486 and Lys85. This figure was drawn using Chimera.(55) For convenience, amino acids are described by a one-letter code, instead of the three-letter code used in the main text.

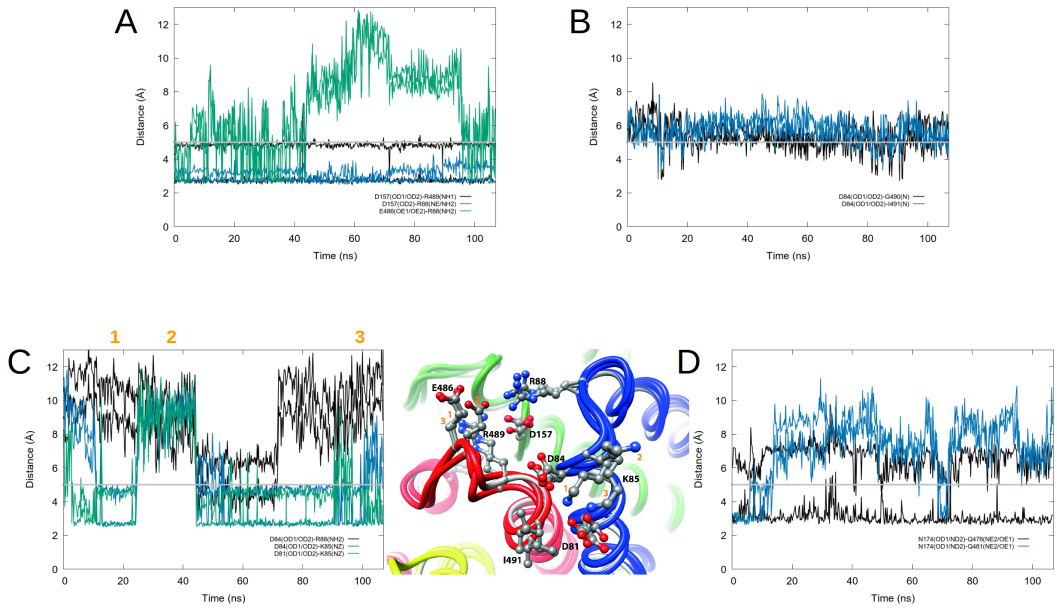

Figure 5. Cell surface expression and iron export ability of the Gln478Ala mutant.

(A) HEK293T cells were transiently transfected with the bicistronic pIRES2 plasmid encoding both full-length human ferroportin 1 and the cluster of differentiation antigen 8 (CD8). After 36h, cells were double-stained for CD8 (APC) and the FPN1-V5 fusion protein (FITC) and analyzed by 2-color flow cytometry. Data are presented as percentage of FPN1-positive over CD8-positive events. Each bar represents the mean ± standard deviation of 3 independent experiments. (B) HEK293T cells were transfected with pcDNA3.1-FPN1-V5-His vectors, grown for 24h00, and then fed with 20μg/mL of ^{55}Fe-transferrin for 16h. Cells were then washed and counted. Counts per minute (cpm) were normalized by total protein and β–Gal activity. Each bar represents the mean ± standard deviation of 5 independent experiments. P values were calculated on Student t-test; ***P*<0.01 compared with wild type FPN1.

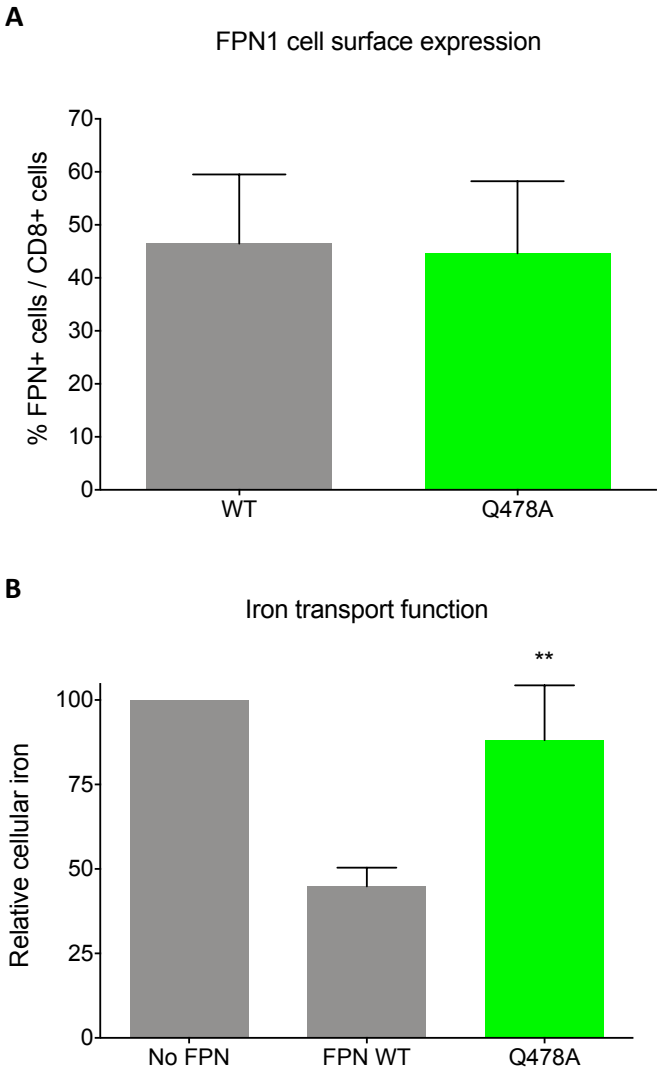

Figure 6. Distribution of iron parameters among suspected hemochromatosis type 4A patients with a missense mutation affecting an FPN1 gating residue.

Serum ferritin and transferrin saturation (when available) values were extracted from the literature for 11 missense mutations (listed in the Table) and 67 patients. Data are presented by gender, since penetrance of the hemochromatosis type 4A-related genotypes at the *SLC40A1* locus is known to be lower in females.

Figure 6

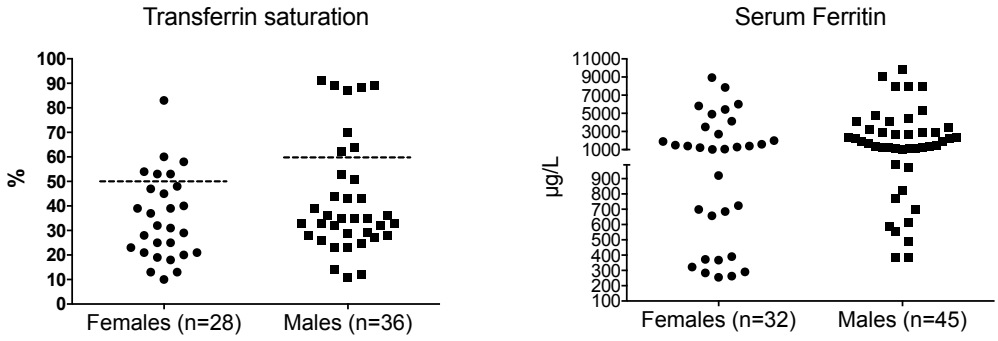

Table 1. List of mutations in the *SLC40A1* gene that affect an FPN1 gating residue.

Mutation	Gender	Age at diagnosis (years)	References
p.Asp84Glu	Female (n=1)	26	(41)
p.Arg88Thr	Female (n=1) Male (n=6)	18 15-61	(42)
p.Arg88Gly	Female (n=2) Male (n=2)	41-77 38-41	(39, 43)
p.Asp157Ala	Female (n=2) Male (n=5)	Not provided 58-66	(44-47, 49)
p.Asp157Gly	Female (n=2) Male (n=2)	42-66 61-64	(39, 48)
p.Asp157Asn	Female (n=4) Male (n=1)	22-76 20	(37, 50)
p.Asp157Tyr	Male (n=1)	64	(39)

p.Asn174Ile	Female (n=2) Male (n=1)	38-66 45	(28, 51)
p.Arg178Gln	Female (n=8) Male (n=17)	11-72 6-71	(15, 43, 52)
p.Arg489Lys	Female (n=4) Male (n=2)	39-60 28-54	(40)
p.Arg489Ser	Male (n=4)	43-81	(46, 53)
p.Gly490Asp	Female (n=4) Male (n=3)	23-54 31-47	(39, 54)
p.Gly490Ser	Female (n=2) Male (n=1)	27-71 24	(39, 43)

Supplementary Data

Supplemental Figure 1.

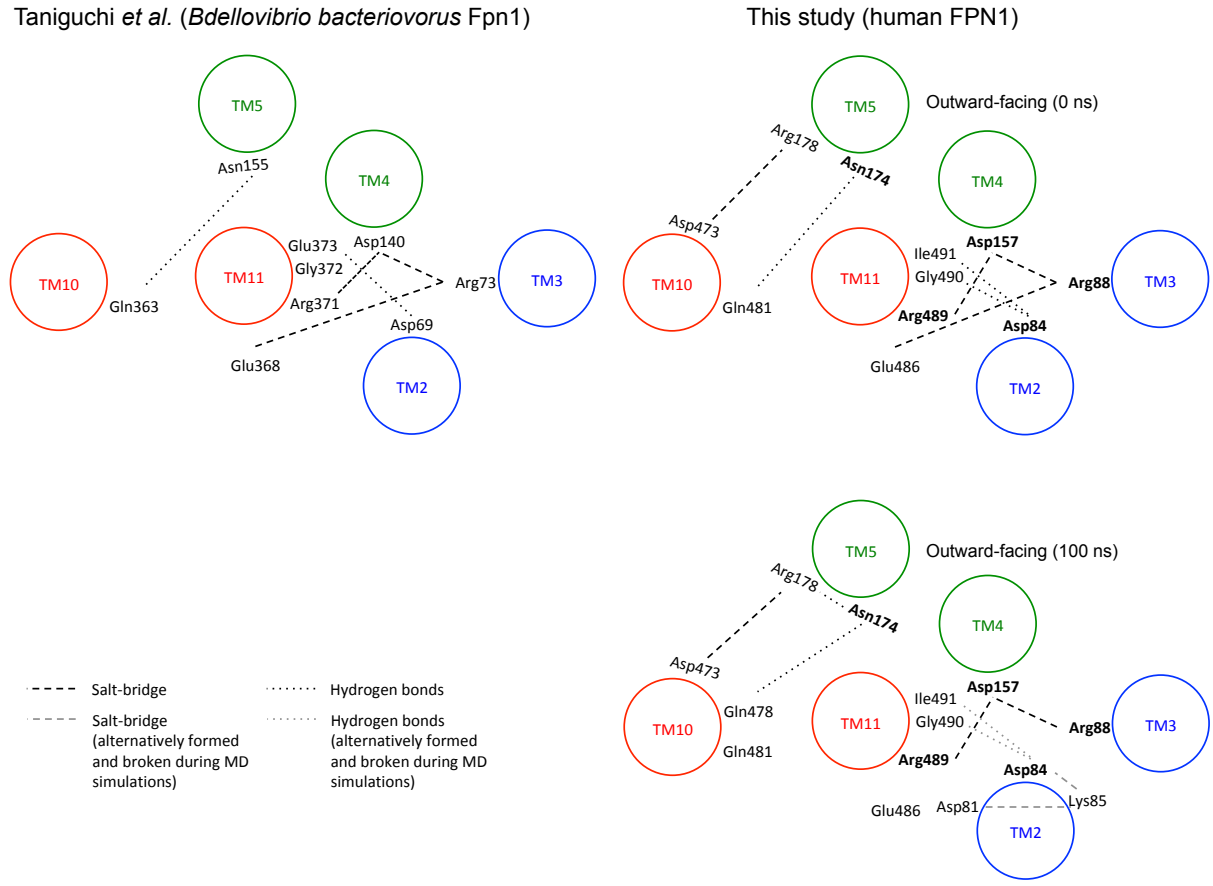

Supplemental Figure 2.

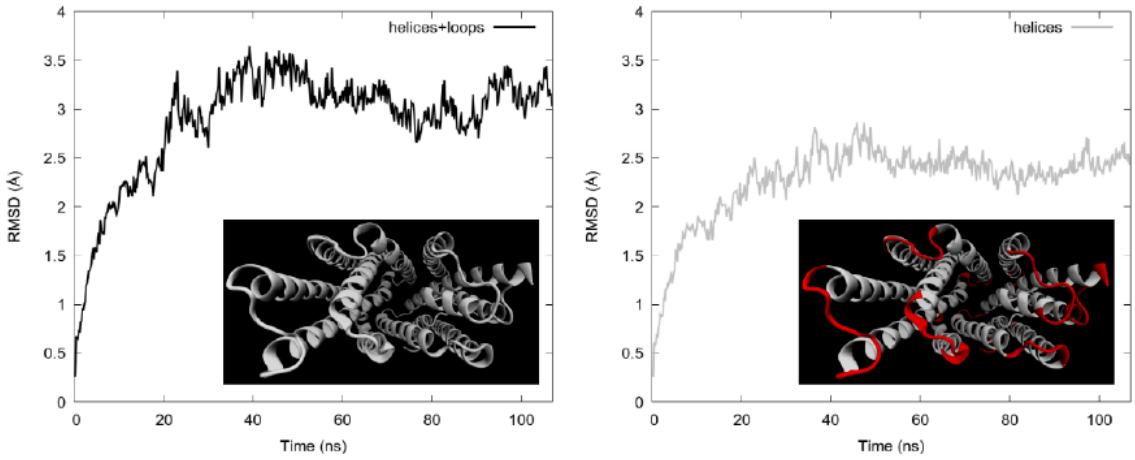

MD simulation (NaCl).

The RMSDs are calculated between the initial model and the simulation snapshots, using the backbone heavy atoms, and plotted as a function of time. In the left panel, RMSDs of the full-length model are plotted whereas in the right panel flexible loops (red regions) were discarded from the analysis.

Supplemental Figure 3.

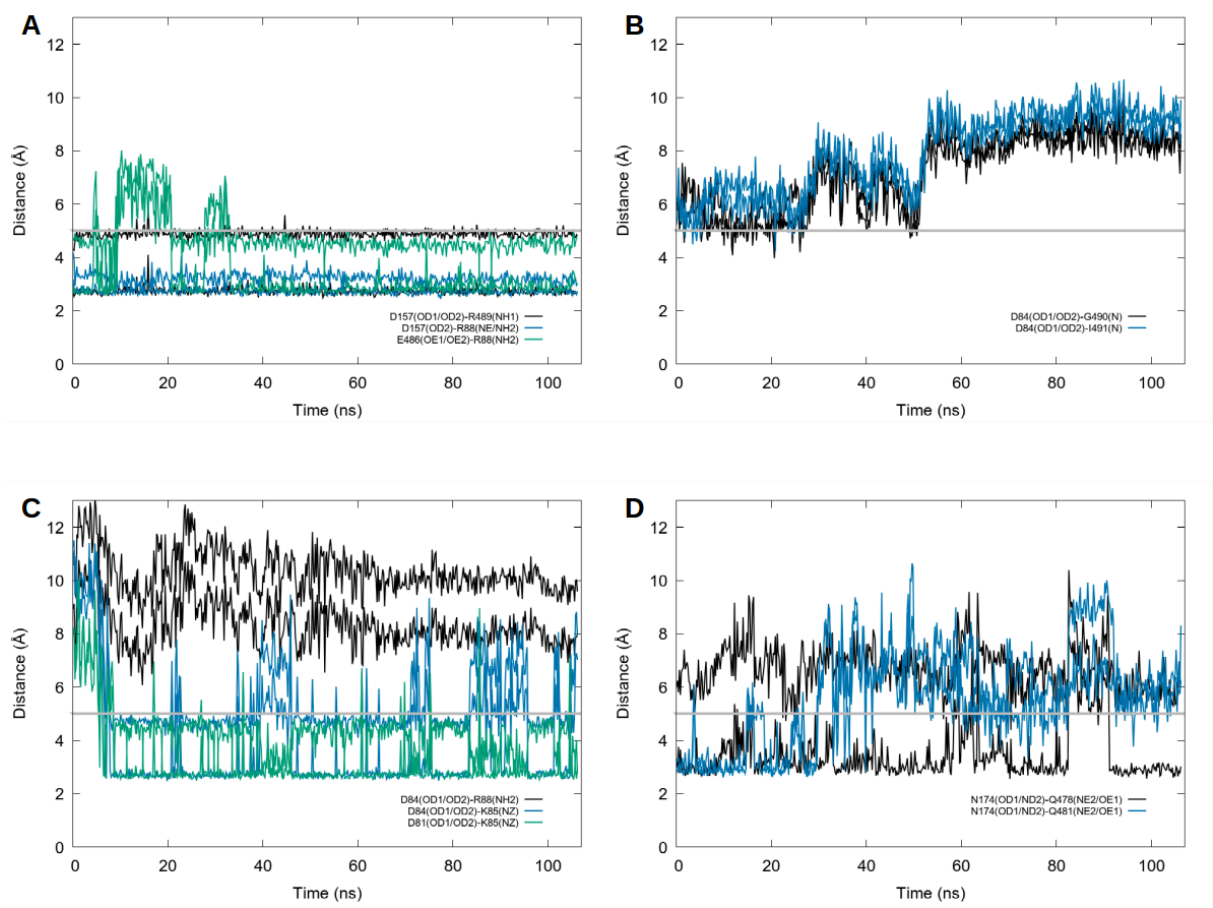

MD simulation ($CaCl^2$).

Distances between atoms involved or not in non-covalent bonds (hydrogen bonds or salt bridges) are plotted as a function of time during the simulation FPN1 model in presence of 70mM of $CaCl^2$.

The plots for the NaCl simulation presented in Figure 1 remain globally similar to these ones, with the following main conclusions : A. a labile (although less pronounced) salt-bridge between E486 and R88 (green line), B. an absence (more pronounced) of H-bonds between D84 and G490/I491, C. the presence of a salt-bridge network involving D81/K85 (blue) and D84/K85 (green), D. a quasi permanent H-bond (black line) between N174 and Q478 (and only occasional one between N174 and Q481, blue line).